



# Heterogeneous nucleation in Zr-Cu-Al-Ag metallic glasses triggered by quenched-in metastable crystals - A time-resolved neutron diffraction study

Zhenduo Wu<sup>a</sup>, Si Lan<sup>a,b</sup>, Xiaoya Wei<sup>a</sup>, Daniel Olds<sup>c</sup>, Katharine Page<sup>c</sup>, Baolong Shen<sup>d</sup>,  
Xun-Li Wang<sup>a,e,\*</sup>

<sup>a</sup> Department of Physics, City University of Hong Kong, 83 Tat Chee Ave., Hong Kong SAR, China

<sup>b</sup> Herbert Gleiter Institute of Nanoscience, Nanjing University of Science and Technology, 200 Xiaolingwei Avenue, Nanjing, Jiangsu, 210094, China

<sup>c</sup> Neutron Scattering Division, Oak Ridge National Laboratory, Oak Ridge, TN, 37831, USA

<sup>d</sup> College of Materials Science and Engineering, Southeast University, Nanjing, 210096, China

<sup>e</sup> Center for Neutron Scattering, City University of Hong Kong Shenzhen Research Institute, 8 Yuexing 1st Road, Shenzhen Hi-Tech Industrial Park, Shenzhen, 518057, China

## ARTICLE INFO

### Keywords:

Neutron scattering  
Bulk metallic glass  
Crystallization  
Heterogeneous nucleation

## ABSTRACT

Crystallization of Zr-Cu-Al-Ag bulk metallic glasses containing quenched-in crystals was studied by time-resolved in-situ neutron diffraction during isothermal annealing in the supercooled liquid region. The quenched-in crystals grew slowly at the beginning, indicating good thermal stability of the Zr-Cu-Al-Ag metallic glass alloys. The neutron diffraction results demonstrated that crystallization in Zr-Cu-Al-Ag metallic glasses was triggered by quenched-in crystals, rather than traditional heterogeneous nucleation mechanisms such as atomic-level impurities, container wall or surface oxides.

## 1. Introduction

The intrinsic glass forming ability (GFA) of a metallic liquid is governed by its homogeneous nucleation behavior [1,2]. However, in many practical cases, heterogeneous nucleation controls the crystallization process during glass formation. For example, the presence of oxides has been proven to trigger heterogeneous nucleation and has a strong negative impact on the GFA of Zr-based bulk metallic glasses (BMGs) [3–6]. Moreover, the fabrication processes of BMGs introduce unavoidable contaminants, such as atomic-level impurities, surface oxides, and quenched-in crystals (QICs). Therefore, heterogeneous nucleation sometimes dominates the nucleation behavior when the BMGs are heated up to their supercooled liquid region [7,8], influencing the thermoplastic formability of the BMGs. In the 1980s, Toloui et al. studied the effect of QICs on the thermal stability of partially amorphous ZrNi alloy. They reported that QICs increase the stability of the amorphous matrix against further crystallization. The pre-existing crystals showed little further growth during heat treatment, and there was no evidence that they acted as heterogeneous nucleation sites [9]. Recently, Yu et al. studied the effects of atomic-level impurities on the thermal stability of Pd<sub>40</sub>Ni<sub>40</sub>P<sub>20</sub> BMG in the supercooled liquid region by state-of-the-art atom probe tomography combined with transmission electron microscopy [10]. They

found that minor impurities dramatically influence the stability of supercooled liquids by changing the heterogeneous crystallization behavior of metallic glasses. Despite its importance, direct studies of details of heterogeneous nucleation in metallic glasses are rare. How these impurities affect the crystallization behavior of metallic glasses in the supercooled liquid region is still not clear and seems to vary from case to case. In this work, capitalizing on the fast data rate enabled by high-flux neutron sources, we performed time-resolved neutron diffraction experiments [11] to study the crystallization behavior of a series of Zr<sub>46</sub>Cu<sub>46-x</sub>Al<sub>8</sub>Ag<sub>x</sub> (x = 6, 8, 10, 12) BMGs (hereafter referred to as Ag6, Ag8, Ag10, Ag12, respectively) in the supercooled liquid region with the presence of a small amount of QICs. According to literature [12], Ag8 has the best GFA (about 20 mm), while Ag12 has the poorest GFA (about 10 mm), among the compositions studied.

## 2. Experiment

Zr-Cu-Al-Ag BMGs of rod shape with a diameter of 3 mm were prepared by Cu-mold casting following the same fabrication process. A relatively slower cooling rate was applied to introduce QICs. The rods were cut and their surfaces were mechanically polished. X-ray diffraction measurements were carried out to characterize the quality of the

\* Corresponding author. Department of Physics, City University of Hong Kong, 83 Tat Chee Ave., Hong Kong SAR, China.  
E-mail address: [xlwang@cityu.edu.hk](mailto:xlwang@cityu.edu.hk) (X.-L. Wang).

samples. Small Bragg peaks were found in the diffraction pattern confirming the presence of a small amount of QICs. Samples with QICs were chosen for Differential Scanning Calorimetry (DSC) and in-situ neutron scattering experiments. The DSC experiment was performed by Netzsch Pegasus DSC at a heating rate of 20 K/min. The neutron scattering experiments were conducted at the NOMAD beamline [13] at the Spallation Neutron Source [14], Oak Ridge National Laboratory, USA. All specimens were isothermally annealed at 15 K above the glass transition temperature for up to 7 h for the measurements. A time resolution of 2 min/pattern was utilized.

### 3. Results

The DSC result for Ag8 is shown in Fig. 1. A clear glass transition around 708 K, marked by  $T_g$ , is observed, followed by an exothermic crystallization peak,  $T_x$ , at about 770 K. The width of supercooled liquid region is more than 40 K, indicating an excellent thermal stability of the sample. The isothermal annealing temperature, marked by  $T_a$ , is about 25 K below the onset temperature of crystallization.

Fig. 2 shows the structure factor  $S(Q)$  of Ag8 BMG obtained at the NOMAD beamline at room temperature. It shows several broad peaks whose peak heights decay rapidly with increasing  $Q$  (the moment transfer), a typical feature of an amorphous material. An enlarged view of the first three peaks is shown at the upper right corner of Fig. 2. Several small peaks, marked by black arrows, can be found on top of the smooth amorphous pattern. These peaks indicate a small amount of QICs which formed during the fabrication process. Because the crystalline peaks are weak, we were not able to index the specific crystalline phases.

Next, we discuss the crystallization behavior. The BMGs were first heated up to 573 K at a heating rate of 50 K/min. They were held at 573 K for 1 min to stabilize the temperature and heated to 723 K for isothermal annealing. Fig. 3 is the 2-D plot showing the evolution of  $S(Q)$  of the Ag8 BMG with annealing time. The inset in Fig. 3 is an enlarged view of the  $S(Q)$  between  $Q$  of 2.4  $\text{\AA}^{-1}$  and 3.2  $\text{\AA}^{-1}$ . Fig. 3 shows  $S(Q)$  changes in two stages. In the first stage, a sharp diffraction peak at  $Q = 2.9 \text{\AA}^{-1}$ , marked by the red arrow, develops from the onset of annealing. As will be discussed below, this peak comes from QICs. When the annealing time reaches about 45 min, the second stage starts. The intensity of the peak at  $Q = 2.9 \text{\AA}^{-1}$  begins to decrease. Meanwhile, another diffraction peak appears at  $Q = 3.1 \text{\AA}^{-1}$ , marked by the blue arrow. The development of this peak signifies the formation of the final crystalline phase (FCP). A similar behavior was found for all samples in the series, with variation in timescales for incubation and FCP growth.

The evolution of  $S(Q)$  indicates a two-step crystallization process. To obtain a clear view of the development of these two peaks, we integrated

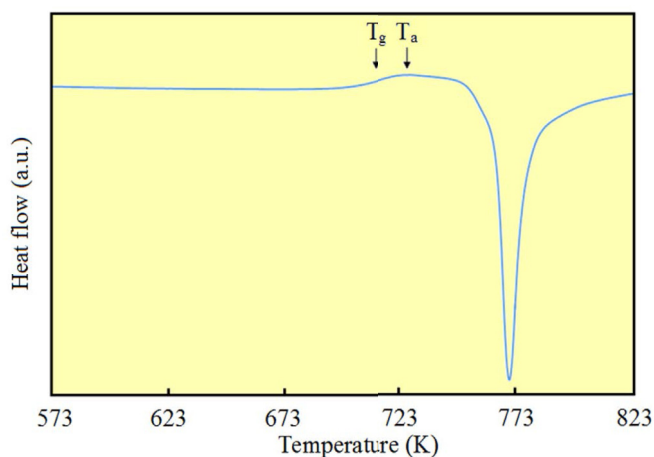


Fig. 1. DSC scan of  $Zr_{46}Cu_{38}Al_8Ag_8$  BMG collected at a heating rate of 20 K/min.  $T_g$  and  $T_a$  are the glass transition temperature and annealing temperature, respectively.

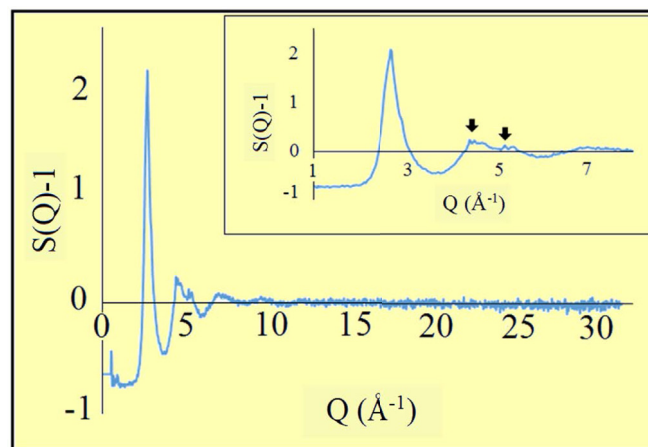


Fig. 2. Room temperature structure factor of the  $Zr_{46}Cu_{38}Al_8Ag_8$  BMG, showing the amorphous structure with a small amount of quenched-in crystalline peaks.

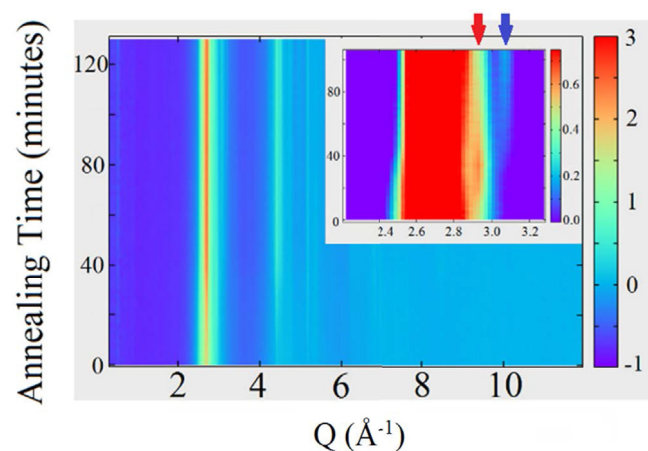


Fig. 3. Evolution of the  $S(Q)$  of  $Zr_{46}Cu_{38}Al_8Ag_8$  BMG with annealing time, collected at 723 K. The quenched-in crystals grow at first as indicated by the red arrow. After about 60 min, the stable crystals appear, as shown by the blue arrow. (For interpretation of the references to colour in this figure legend, the reader is referred to the Web version of this article.)

the intensities of the  $S(Q)$  of four Zr-Cu-Al-Ag BMGs from 2.88  $\text{\AA}^{-1}$  to 2.98  $\text{\AA}^{-1}$  for the diffraction peak from the QICs and from 3.02  $\text{\AA}^{-1}$  to 3.12  $\text{\AA}^{-1}$  for the crystalline peak from the FCP. The results are summarized in Fig. 4 for all samples. In Fig. 4a, the intensity of the QICs starts to rise at the beginning of annealing but the increase halts after  $\sim 70$  min and then the intensity declines. In Fig. 4b, there is no intensity in the region of the FCP peak at first. After an incubation period of 60 min, an FCP peak appears and begins to grow over time. The incubation time of the FCP generally increases with a decreasing amount of Ag content. From Fig. 4, it can be seen that the turning point of the intensity from QICs is roughly the same as the emergence of the FCP for all four BMGs. Ag6 has a significantly longer incubation time for the nucleation of the stable crystalline phase than other BMGs.

Quantitative evaluation of the amorphous-to-crystalline phase transformation was carried out using the combinatorial appraisal of transition states (CATS) software [15]. Assuming that the amorphous states remain the same throughout the annealing, i.e., the  $S(Q)$  of amorphous phase does not change, we can estimate the volume fraction of the remaining amorphous phases during the entire crystallization process, as follows [16],

$$S(Q, t) = f(t)S_a(Q) + [1 - f(t)]S_c(Q),$$

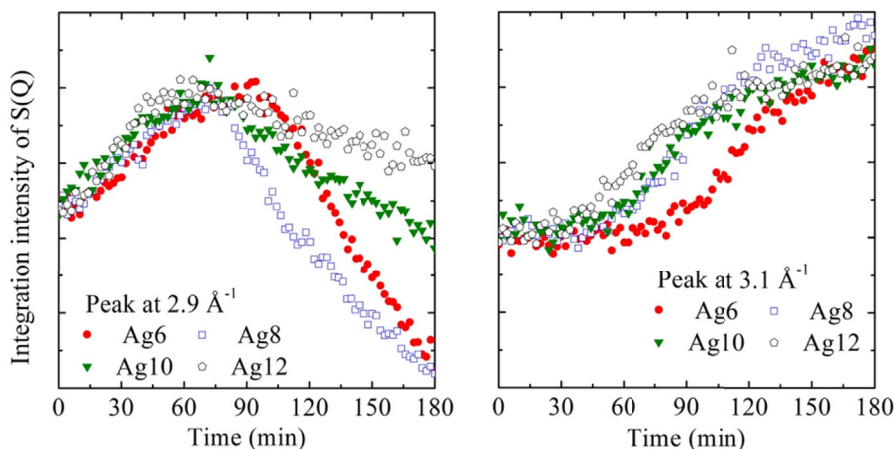


Fig. 4. Integration intensities of  $S(Q)$  for four Zr-Cu-Al-Ag metallic glasses. (a) Diffraction peak at  $Q \sim 2.9 \text{ \AA}^{-1}$  from the quenched-in crystalline phase. It starts to grow at the beginning of annealing and stops growing when the stable crystalline phase forms. (b) Diffraction peak at  $Q \sim 3.1 \text{ \AA}^{-1}$  which arises from the stable final crystalline phase and starts to growing at  $\sim 60$  min. The incubation time of Ag6 can be as long as 80 min.

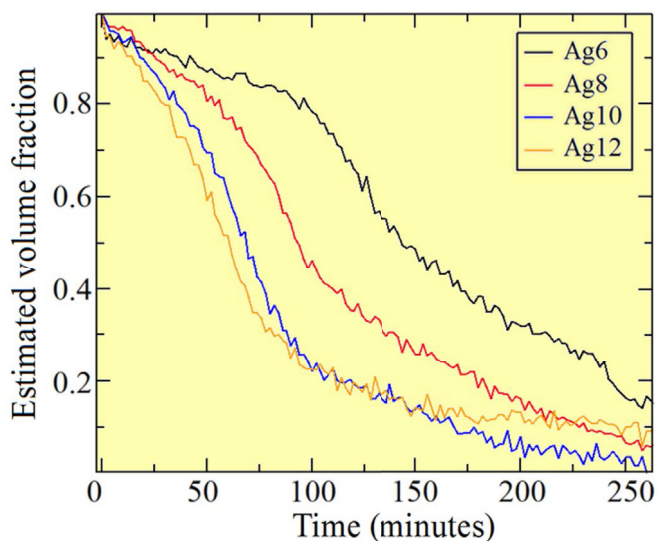


Fig. 5. Volume fraction of the remaining amorphous phase as a function of annealing time.

where  $f(t)$  is the volume fraction of the amorphous phase, and  $S_a(Q)$  and  $S_c(Q)$  are the structure factors for the amorphous phase and FCP, respectively. Assuming that  $S_a(Q)$  and  $S_c(Q)$  do not vary with time, the  $f(t)$  can be calculated and the results are shown in Fig. 5. The amorphous phase starts to decrease slightly at the beginning, which is due to the growth of the QICs. After several minutes, the volume fraction of the QICs shows a sudden drop, which is due to the formation of the stable crystalline phase.

#### 4. Discussion

As shown in Fig. 4, the diffraction intensity at  $Q \sim 2.9 \text{ \AA}^{-1}$  starts to increase without incubation time. It indicates that this peak comes from the QICs. The QICs grow slightly at the initial stage of annealing. On the other hand, the intensity at  $Q \sim 3.1 \text{ \AA}^{-1}$  appears after a certain time, indicating that it comes from a stable crystalline phase that forms during annealing. The excellent correlation of the turning points of peak intensities from Fig. 4 confirms that crystallization of the BMGs is triggered by the QICs, which served as heterogeneous nucleation sites. After the appearance of the stable crystals during annealing, QICs stop growing

and start to disappear. The results indicate that the heterogeneous nucleation in these supercooled Zr-Cu-Al-Ag BMGs is not caused by atomic level impurities, container walls, or surface oxides. Instead, they suggest that QICs play the most important role on the crystallization of the BMGs annealed in the supercooled liquid region. It is quite possible that crystallization takes place at the liquid/crystal interface of the QICs. Once the heterogeneous nucleation completes, the surface of nucleation sites is entirely covered by the new stable crystalline phase, preventing further growth of the QICs. This scenario can explain the decrease of the intensity from the QICs after the final stable crystalline phase is formed. The experiments further demonstrate that the good glass former Zr-Cu-Al-Ag has a very high thermal stability. Ag6 is the most stable sample, with an incubation time for heterogeneous nucleation that can be as long as 80 min at a temperature 15 K above the glass transition.

#### 5. Conclusion

Time resolved in-situ neutron scattering experiments show that the supercooled liquid of Zr-Cu-Al-Ag is very stable even when containing QICs. The QICs grow slowly when annealed at 15 K above  $T_g$ . The QICs dominate the heterogeneous nucleation of the supercooled Zr-Cu-Al-Ag liquid, while traditional mechanisms for heterogeneous nucleation such as atomic level impurities, container walls or surface oxides play less of a role. Our experimental results also show that the BMG with the highest resistance against crystallization (Ag6) is not necessarily the BMG of the highest GFA (Ag8).

#### Acknowledgement

The work described in this paper was supported by a grant from the Research Grants Council of the Hong Kong Special Administrative Region, China [Project No. CityU 11216215]. X.L. Wang and S. Lan acknowledge the support by the National Natural Science Foundation of China (Grant No. 51571170 and 51501090). The neutron scattering experiments were carried out at the Spallation Neutron Source, which is sponsored by the Scientific User Facilities Division, Office of Basic Energy Sciences, U.S. Department of Energy, under contract No. DE-AC05-00OR22725 with Oak Ridge National Laboratory.

#### References

- [1] D. Turnbull, Under what conditions can a glass be formed? *Contemp. Phys.* 10 (5) (1969) 473–488.
- [2] W.L. Johnson, J.H. Na, M.D. Demetriou, Quantifying the origin of metallic glass formation, *Nature Commun.* (2016) 7.

- [3] C.T. Liu, M.F. Chisholm, M.K. Miller, Oxygen impurity and microalloying effect in a Zr-based bulk metallic glass alloy, *Intermetallics* 10 (11) (2002) 1105–1112.
- [4] A. Gebert, J. Eckert, L. Schultz, Effect of oxygen on phase formation and thermal stability of slowly cooled  $Zr_{65}Al_{7.5}Cu_{17.5}Ni_{10}$  metallic glass, *Acta Mater.* 46 (15) (1998) 5475–5482.
- [5] B.S. Murty, D.H. Ping, K. Hono, et al., Influence of oxygen on the crystallization behavior of  $Zr_{65}Cu_{27.5}Al_{7.5}$  and  $Zr_{66.7}Cu_{33.3}$  metallic glasses, *Acta Mater.* 48 (15) (2000) 3985–3996.
- [6] M.W. Chen, A. Inoue, T. Sakurai, et al., Impurity oxygen redistribution in a nanocrystallized  $Zr_{65}Cr_{15}Al_{10}Pd_{10}$  metallic glass, *Appl. Phys. Lett.* 74 (6) (1999) 812–814.
- [7] H.W. Kui, D. Turnbull, Melting of  $Ni_{40}Pd_{40}P_{20}$  glass, *Appl. Phys. Lett.* 47 (8) (1985) 796–797.
- [8] J. Schroers, A. Masuhr, W.L. Johnson, et al., Pronounced asymmetry in the crystallization behavior during constant heating and cooling of a bulk metallic glass-forming liquid, *Phys. Rev. B* 60 (17) (1999) 11855.
- [9] B. Toloui, G. Grogan, M.G. Scott, The influence of quenched-in crystals on the thermal stability of partially amorphous  $Zr_{76}Ni_{24}$  alloy, *J. Mater. Sci.* 19 (1984) 4007–4013.
- [10] J.S. Yu, Y.Q. Zeng, T. Fujita, et al., On the effect of impurities in metallic glass formation, *Appl. Phys. Lett.* 96 (14) (2010), 141901.
- [11] S. Lan, X. Wei, J. Zhou, et al., In-situ study of crystallization kinetics in ternary bulk metallic glass alloys with different glass forming abilities, *Appl. Phys. Lett.* 105 (20) (2014), 201906.
- [12] W. Zhang, Q. Zhang, C. Qin, et al., Synthesis and properties of Cu–Zr–Ag–Al glassy alloys with high glass-forming ability, *Mater. Sci. Eng. B* 148 (1) (2008) 92–96.
- [13] Jörg Neuefeind, Mikhail Feygenson, John Carruth, Ron Hoffmann, Kenneth K. Chipley, The nanoscale ordered MATERIALS diffractometer NOMAD at the spallation neutron source SNS, *Nucl. Instrum. Methods Phys. Res. Sect. B Beam Interact. Mater. Atoms* 287 (2012) 68–75.
- [14] T.E. Mason, D. Abernathy, I. Anderson, J. Ankner, T. Egami, G. Ehlers, A. Ekkebus, G. Granroth, M. Hagen, K. Herwig, J. Hodges, C. Hoffmann, C. Horak, L. Horton, F. Klose, J. Larese, A. Mesecar, D. Myles, J. Neuefeind, M. Ohl, C. Tulk, X.-L. Wang, J. Zhao, The spallation neutron source in Oak Ridge: a powerful tool for materials research, *Phys. B* 385–386 (2006) 955–960.
- [15] Olds Daniel, Peter F. Peterson, Michael K. Crawford, et al., Combinatorial appraisal of transition states for in situ pair distribution function analysis, *J. Appl. Cryst.* 50 (6) (2017) 1744–1753.
- [16] D. Ma, A.D. Stoica, X.L. Wang, Z.P. Lu, et al., In-situ neutron scattering study of crystallization in a Zr-based bulk metallic glass, *Appl. Phys. A Mater. Sci. Proc.* 99 (3) (2010) 537–542.